Phys. Proc. Ultra-Peripheral Collisions **1**, 009 (2024) 1-9

Impact parameter dependence of dilepton production: Wigner function approach and the role of photon polarizations

Wolfgang Schäfer
Institute of Nuclear Physics, Polish Academy of Sciences,
ul. Radzikowskiego 152, PL-31-342 Kraków, Poland

We revisit the Wigner function approach to the impact parameter dependent dilepton pair production developed in [M. Klusek-Gawenda, WS, A. Szczurek Phys.Lett.B 814 (2021) 136114]. We study the distribution of the angle between difference and sum of lepton transverse momenta, and show how it relates to the orbital angular momentum of leptons. The dependence on impact paramter is discussed, and we also present the different components of the Wigner function in the t-channel. A brief comparison to similar angular distributions in diffractive quark pair production will be presented.

DOI: https://doi.org/10.17161/werm5m52
Keywords: UPC, dileptons, Wigner function

1 Introduction

The uses of Weizsäcker-Williams (WW) photons in ultraperipheral collisions of heavy ions [1,2,3,4] need no introduction at this conference. Here, we will concentrate on the role of WW-photons in peripheral to semi-central processes, where nuclei overlap in impact parameter space and interact strongly. This can include the production of quark-gluon plasma in the nuclear overlap region. For our purposes the additional strong interactions create an "underlying event" to the $\gamma\gamma$-process induced by the WW-photons. The possibility of extending the WW approach to such inelastic collisions has been realized already in the 1990s [5], but has become topical after the measurements by the STAR collaboration at RHIC of J/ψ [6] and dielectrons [7] at very low transverse momenta of the produced system. Below, we concentrate on lepton pair production. In fact it is straightforward to write the relevant cross section in impact parameter space, involving a convolution of the $\boldsymbol{b}$–dependent photon fluxes:

$$\frac{d\sigma_{ll}}{d\xi d^2\boldsymbol{b}} = \int d^2\boldsymbol{b}_1 d^2\boldsymbol{b}_2\, \delta^{(2)}(\boldsymbol{b}-\boldsymbol{b}_1-\boldsymbol{b}_2) N(\omega_1, b_1) N(\omega_2, b_2) \frac{d\sigma(\gamma\gamma\to l^+l^-;\hat{s})}{d(-\hat{t})} \,, \tag{1}$$

where the phase space element is $d\xi = dy_+ dy_- dp_T^2$ with $y_\pm$, p_T and m_l the *single-lepton* rapidities, transverse momentum and mass, respectively, and

$$\omega_1 = \frac{\sqrt{p_T^2+m_l^2}}{2}\left(e^{y_+}+e^{y_-}\right) \,,\ \omega_2 = \frac{\sqrt{p_T^2+m_l^2}}{2}\left(e^{-y_+}+e^{-y_-}\right) \,,\ \hat{s} = 4\omega_1\omega_2 \,. \tag{2}$$

It is then straightforward to evaluate the cross sections/yields for different centrality classes $\mathcal{C}$, which are slices in impact parameter space $[b_{\rm min}, b_{\rm max}]$ that contain a fraction $f_{\mathcal{C}}$ of the total inelastic cross section $\sigma^{\rm in}_{\rm AA}$. For example

$$\frac{dN_{ll}[\mathcal{C}]}{dM} = \frac{1}{f_{\mathcal{C}}\cdot\sigma^{\rm in}_{\rm AA}} \int_{b_{\rm min}}^{b_{\rm max}} db \int d\xi\, \delta(M-2\sqrt{\omega_1\omega_2}) \frac{d\sigma_{ll}}{d\xi db}\Big|_{\rm cuts}. \tag{3}$$

Up to now we have treated WW photons as purely collinear partons of the ions, in particular the dilepton pair is produced back–to–back with a delta-function distribution of the pair transverse momentum. An excellent agreement with the invariant mass distributions of dileptons with $P_T < 150\,$MeV for the most

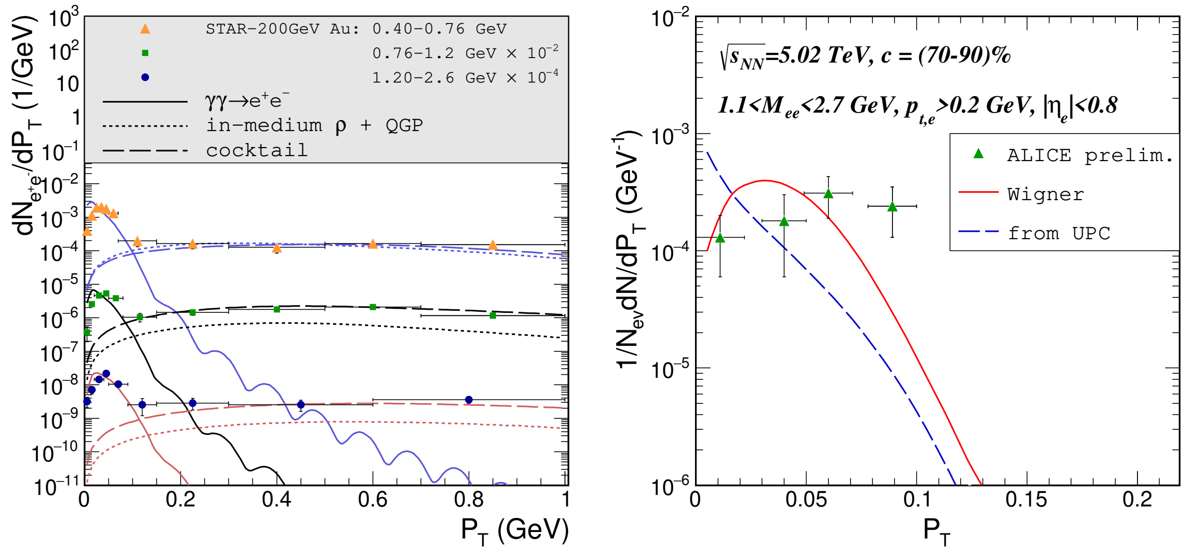

Figure 1 – Left panel: P_T spectra of the individual contributions in 3 different mass bins for 60-80% central Au+Au collisions ($\sqrt{s_{NN}}$=200 GeV), compared to STAR data [7]. Right panel: P_T distribution of the pair against old preliminary ALICE data [8].

peripheral STAR data is achieved in such an approach [9]. For more central collisions also thermal emissions and the cocktail of hadronic Dalitz as described in Ref.[10] decays plays a role.

The proof for the presence of the photon fusion mechanism however lies in the pair-transverse momentum distribution. One can easily obtain the transverse momentum dependent WW-flux of photons, which reads

$$\frac{dN(\omega,\boldsymbol{q})}{d^2\boldsymbol{q}} = \frac{Z^2\alpha_{\rm em}}{\pi^2}\frac{\boldsymbol{q}^2}{[\boldsymbol{q}^2+\frac{\omega^2}{\gamma^2}]^2}F^2_{\rm em}(\boldsymbol{q}^2+\frac{\omega^2}{\gamma^2}). \tag{4}$$

Here the electromagnetic formfactor of the nucleus restricts transverse momenta to $\boldsymbol{q}^2 \lesssim 6/R_A^2$, while the maximum of the distribution is at $\boldsymbol{q}^2 \sim \omega^2/\gamma^2$, which takes smaller values with increasing Lorentz factor γ. The dilepton cross section is then written as

$$\frac{d\sigma_{ll}}{d^2\boldsymbol{P}} = \int \frac{d\omega_1}{\omega_1}\frac{d\omega_2}{\omega_2} d^2\boldsymbol{q}_1 d^2\boldsymbol{q}_2 \frac{dN(\omega_1,\boldsymbol{q}_1^2)}{d^2\boldsymbol{q}_1}\frac{dN(\omega_2,\boldsymbol{q}_2^2)}{d^2\boldsymbol{q}_2}\delta^{(2)}(\boldsymbol{q}_1+\boldsymbol{q}_2-\boldsymbol{P})\hat{\sigma}(\gamma\gamma\to l^+l^-)\Big|_{\rm cuts}, \tag{5}$$

so that the transverse momentum distribution of the dilepton *pair* is essentially obtained by a convolution of WW-fluxes. This of course closely reminds the TMD (transverse momentum dependent) factorization formulas used in inclusive hadronic processes. The similarity would be even more obvious by using momentum fractions $x_i = 2\omega_i/\sqrt{s_{\rm NN}}$ instead of photon energies. A similar procedure is taken in the Monte-Carlo code Starlight [11]. In the left panel of Fig.1 we show the comparison of a calculation based on eq.5 with STAR data. Closer inspection shows, that the peak however is predicted at smaller P_T than what data show. This disagreement becomes rather dramatic at LHC energies, see the right panel of Fig.1. Here the blue dashed line reflects the ever smaller transverse momenta of photons at higher energies.

2 Wigner function approach

2.1 Wigner function & factorization

As it turns out it is crucial to include simultaneously the dependence on centrality/impact parameter of the collision and the pair transverse momentum [12].

$$N_{ij}(\omega,\boldsymbol{b},\boldsymbol{q}) = \int \frac{d^2\boldsymbol{Q}}{(2\pi)^2}\exp[-i\boldsymbol{b}\boldsymbol{Q}]\,E_i\Big(\omega,\boldsymbol{q}+\frac{\boldsymbol{Q}}{2}\Big)E_j^*\Big(\omega,\boldsymbol{q}-\frac{\boldsymbol{Q}}{2}\Big). \tag{6}$$

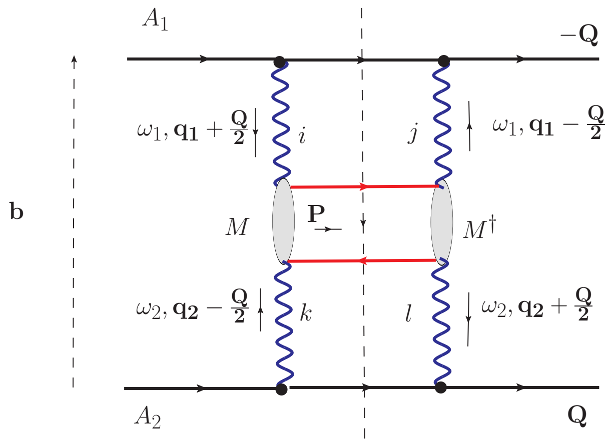

Figure 2 – Diagrammatic representation of the factorization formula for the cross section at fixed impact parameter of the colliding particles. It is related to the cut of a non-forward elastic amplitude.

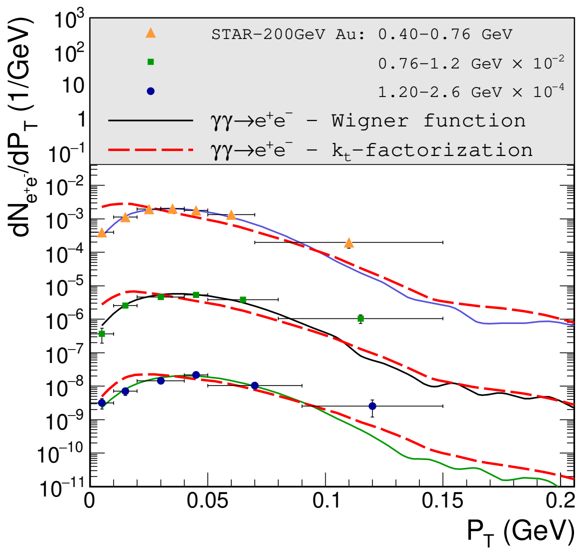

Figure 3 – P_T spectra for 60-80% central Au+Au collisions ($\sqrt{s_{\rm NN}}$=200 GeV) Calculations from Ref.[12].

Above, we introduced the electric field strength vector

$$\boldsymbol{E}(\omega, \boldsymbol{q}) \propto \frac{\boldsymbol{q} F_{\rm em}(\boldsymbol{q}^2 + \frac{\omega^2}{\gamma^2})}{\boldsymbol{q}^2 + \frac{\omega^2}{\gamma^2}}. \tag{7}$$

The Wigner function depends at the same time on impact parameter and transverse momentum, and will reproduce the above mention WW fluxes in impact parameter and transverse momentum space after being integrated over the respective other set of variables. It is also a density matrix in photon polarizations – above indices i, j correspond to cartesian (linear) polarizations of WW photons. The relation to the operator matrix element definition is shown in Ref.[13]. For earlier approaches to the impact parameter dependence, see e.g. Ref.[14] (which does not discuss the pair P_T-spectrum and photon polarizations) and Ref.[15], which is based on a numerical Fourier transform of Feynman-diagram amplitudes. For an equivalent approach to ours and a discussion of soft-photon resummation [16], see the presentation by Ya-Jin Zhou at this workshop. For the analogous QCD Wigner function of gluons with applications to mainly exclusive processes we refer to the recent review [17]. The factorization formula differs from the standard expressions in several aspects, the most important being the fact that here it is not the hard cross section averaged over incoming parton polarizations that enters, but rather a mixture of incoming polarizations is prepared dependent on $\boldsymbol{b}$.

$$\begin{aligned}\frac{d\sigma}{d^2\boldsymbol{b}d^2\boldsymbol{P}} &= \int d^2\boldsymbol{b}_1 d^2\boldsymbol{b}_2\, \delta^{(2)}(\boldsymbol{b}-\boldsymbol{b}_1+\boldsymbol{b}_2) \int \frac{d\omega_1}{\omega_1}\frac{d\omega_2}{\omega_2} d^2\boldsymbol{q}_1 d^2\boldsymbol{q}_2\, \delta^{(2)}(\boldsymbol{P}-\boldsymbol{q}_1-\boldsymbol{q}_2) \\ &\times\; N_{ij}(\omega_1,\boldsymbol{b}_1,\boldsymbol{q}_1)N_{kl}(\omega_2,\boldsymbol{b}_2,\boldsymbol{q}_2)\, \frac{1}{2\hat{s}} M_{ik}M^\dagger_{jl}\, d\Phi(l^+l^-). \end{aligned} \tag{8}$$

For a diagrammatic representation, see Fig.2. For practical calculations it is useful to start from the more explicit form

$$\begin{aligned}\frac{d\sigma}{d^2\boldsymbol{b}d^2\boldsymbol{P}} &= \int \frac{d^2\boldsymbol{Q}}{(2\pi)^2}\exp[-i\boldsymbol{b}\boldsymbol{Q}] \int \frac{d\omega_1}{\omega_1}\frac{d\omega_2}{\omega_2}\int\frac{d^2\boldsymbol{q}_1}{\pi}\frac{d^2\boldsymbol{q}_2}{\pi}\,\delta^{(2)}(\boldsymbol{P}-\boldsymbol{q}_1-\boldsymbol{q}_2) \\ &\times\; E_i\Big(\omega_1,\boldsymbol{q}_1+\frac{\boldsymbol{Q}}{2}\Big)E^*_j\Big(\omega_1,\boldsymbol{q}_1-\frac{\boldsymbol{Q}}{2}\Big)E_k\Big(\omega_2,\boldsymbol{q}_2-\frac{\boldsymbol{Q}}{2}\Big)E^*_l\Big(\omega_2,\boldsymbol{q}_2+\frac{\boldsymbol{Q}}{2}\Big) \\ &\times\; \frac{1}{2\hat{s}}\sum_{\lambda\bar\lambda} M^{\lambda\bar\lambda}_{ik}M^{\lambda\bar\lambda\dagger}_{jl}\, d\Phi(l^+l^-). \end{aligned}$$

with

$$\begin{aligned}\sum_{\lambda\bar\lambda} M^{\lambda\bar\lambda}_{ik}M^{\lambda\bar\lambda\dagger}_{jl} &= \delta_{ik}\delta_{jl}\sum_{\lambda\bar\lambda}\Big|M^{(0,+)}_{\lambda\bar\lambda}\Big|^2 + \epsilon_{ik}\epsilon_{jl}\sum_{\lambda\bar\lambda}\Big|M^{(0,-)}_{\lambda\bar\lambda}\Big|^2 \\ &+\; P^{\parallel}_{ik}P^{\parallel}_{jl}\sum_{\lambda\bar\lambda}\Big|M^{(2,-)}_{\lambda\bar\lambda}\Big|^2 + P^{\perp}_{ik}P^{\perp}_{jl}\sum_{\lambda\bar\lambda}\Big|M^{(2,+)}_{\lambda\bar\lambda}\Big|^2 + \text{interferences}\,. \end{aligned} \tag{9}$$

Here, the mutually orthogonal $O(2)$-tensors

$$\delta_{ik} = \hat{x}_i\hat{x}_k+\hat{y}_i\hat{y}_k,\;\; \epsilon_{ik}=\hat{x}_i\hat{y}_k-\hat{y}_i\hat{x}_k,\;\; P^{\parallel}_{ik}=\hat{x}_i\hat{x}_k-\hat{y}_i\hat{y}_k,\;\; P^{\perp}_{ik}=\hat{x}_i\hat{y}_k+\hat{y}_i\hat{x}_k \tag{10}$$

project the incoming (s-channel) photon polarization states into definite $J_z = 0, \pm 2$ and parity. In Fig.3 we see that the inclusion of the impact parameter dependence within the Wigner function approach gives an improved description of STAR data with no new parameters introduced. Other successes[12] include a good description of the evolution of azimuthal decaorrelation of dileptons with centrality, as measured by the ATLAS Collaboration [18].

2.2 Positivity

The form of the cross section given in eq.9 also gives straightforward insight into positivity issues. Namely the Wigner function is not necessarily a non-negative function. One may therefore doubt, whether our cross section is manifestly positive, i.e. well-defined. To this end, we can introduce:

$$G_{ik}(\omega_1,\omega_2,\boldsymbol{P};\boldsymbol{b}) \equiv \int \frac{d^2\boldsymbol{k}}{2\pi^2}\exp[-i\boldsymbol{b}\boldsymbol{k}]\, E_i(\omega_1,\boldsymbol{k})E_k(\omega_2,\boldsymbol{P}-\boldsymbol{k})\,, \tag{11}$$

so that our cross section takes the form

$$\frac{d\sigma}{d^2\boldsymbol{b}d^2\boldsymbol{P}} = \int \frac{d\omega_1}{\omega_1}\frac{d\omega_2}{\omega_2} G_{ik}(\omega_1,\omega_2,\boldsymbol{P};\boldsymbol{b})G^*_{jl}(\omega_1,\omega_2,\boldsymbol{P};\boldsymbol{b})\,\frac{1}{2\hat{s}}\sum_{\lambda\bar\lambda}M^{\lambda\bar\lambda}_{ik}M^{\lambda\bar\lambda\dagger}_{jl}\,d\Phi(l^+l^-)\,. \tag{12}$$

from which we obtain the cross section as a sum of squares which is manifestly positive:

$$\begin{aligned}\frac{d\sigma}{d^2\boldsymbol{b}d^2\boldsymbol{P}} &= \int\frac{d\omega_1}{\omega_1}\frac{d\omega_2}{\omega_2}\Big\{|G_{xx}+G_{yy}|^2\sum_{\lambda\bar\lambda}\Big|M^{(0,+)}_{\lambda\bar\lambda}\Big|^2 + |G_{xy}-G_{yx}|^2\sum_{\lambda\bar\lambda}\Big|M^{(0,-)}_{\lambda\bar\lambda}\Big|^2 \\ &+\; |G_{xx}-G_{yy}|^2\sum_{\lambda\bar\lambda}\Big|M^{(2,+)}_{\lambda\bar\lambda}\Big|^2 + |G_{xy}+G_{yx}|^2\sum_{\lambda\bar\lambda}\Big|M^{(2,-)}_{\lambda\bar\lambda}\Big|^2\Big\}\frac{d\Phi(l^+l^-)}{2\hat{s}}\,. \end{aligned} \tag{13}$$

2.3 Fierz transformation & t-channel viewpoint

While positivity is easiest proven from the s-channel point of view, it is of interest to analyze which components of the spin-density matrix of the beam/target nuclei are being probed by the “hard process”

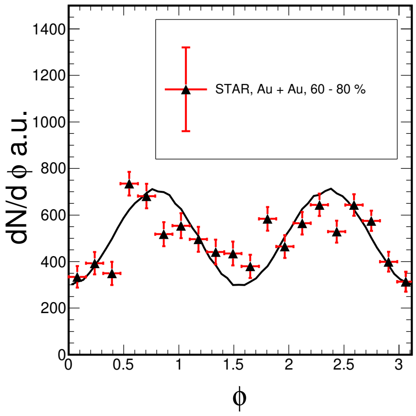

Figure 4 – Data from STAR [20],experimental cuts: $0.45 < M < 0.76$ GeV, $P_T < 0.1$ GeV.

under discussion. Here one often uses the generalized transverse momentum distributions (GTMDs), which are derived from the Wigner distributions by another Fourier transform (see the e.g. the review[17]):

$$\mathcal{G}_{ij}(x,\boldsymbol{q},\boldsymbol{Q}) \propto \int d^2\boldsymbol{b}\, \exp[i\boldsymbol{b}\boldsymbol{Q}]\, N_{ij}(x,\boldsymbol{b},\boldsymbol{q})\,. \tag{14}$$

While it would be perhaps most convenient to decompose the GTMD/density matrix in terms of the orthogonal $O(2)$ tensors given above, popular parametrizations (see e.g.[19]) use decompositions like

$$\begin{aligned}\mathcal{G}_{ij}(x,\boldsymbol{q},\boldsymbol{Q}) &= \delta_{ij}\mathcal{G}_1(x,\boldsymbol{q},\boldsymbol{Q}) + (2q_iq_j - \boldsymbol{q}^2\delta_{ij})\mathcal{G}_2(x,\boldsymbol{q},\boldsymbol{Q}) \\ &+ (2Q_iQ_j - \boldsymbol{Q}^2\delta_{ij})\mathcal{G}_3(x,\boldsymbol{q},\boldsymbol{Q}) + (q_iQ_j - Q_iq_j)\mathcal{G}_4(x,\boldsymbol{q},\boldsymbol{Q}),\end{aligned} \tag{15}$$

where in fact for small-x photons all the GTMDs are proportional to each other. In the forward limit $\boldsymbol{Q} \to 0$, which corresponds to the integration over impact parameters in the Wigner function, we have the TMD limits $\mathcal{G}_1 \to f_1(x,\boldsymbol{q})$, $\mathcal{G}_2 \to h_1^\perp(x,\boldsymbol{q})$, where f_1 and $h_1^\perp$ are the TMD for unpolarized and linearly polarized photons repsectively.. To convert the sums over polarizations in Eq.9, one may use a "Fierz transformation" which swaps contractions $P_{ik}P_{jl}$ to $P_{ij}P_{kl}$:

$$\left.\begin{pmatrix} \mathbb{I}\otimes\mathbb{I} \\ \varepsilon\otimes\varepsilon \\ P^{\parallel}\otimes P^{\parallel} \\ P^{\perp}\otimes P^{\perp}\end{pmatrix}\right|_{s-\text{channel}} = \frac{1}{2}\begin{pmatrix} 1 & 1 & 1 & 1 \\ 1 & 1 & -1 & -1 \\ 1 & -1 & 1 & -1 \\ 1 & -1 & -1 & 1\end{pmatrix}\left.\begin{pmatrix} \mathbb{I}\otimes\mathbb{I} \\ \varepsilon\otimes\varepsilon \\ P^{\parallel}\otimes P^{\parallel} \\ P^{\perp}\otimes P^{\perp}\end{pmatrix}\right|_{t-\text{channel}} \tag{16}$$

2.4 Polarization structure & angular dependence

Before we come to the angular dependence of the cross section, let us briefly look at helicity amplitudes of leptons in states of definite J_z and parity. As it turns out, all amplitudes with $J_z = 0$ vanish in the limit of massless fermions. We work in terms of light-front momentum fractions $z, 1-z$ of one of the photons carried by the (anti-)lepton and the relative transverse momentum

$$\boldsymbol{k} = z\boldsymbol{p}_- - (1-z)\boldsymbol{p}_+\,. \tag{17}$$

As the total angular momentum is decomposed into spin and orbital angular momentum $J_z = S_z + L_z$, amplitudes will have dependences on the azimuthal angle ϕ of $\boldsymbol{k}$ which involve

$$\exp(\pm iL_z\phi) = \exp(\pm i(J_z - S_z)\phi). \tag{18}$$

For example, the positive parity, $J_z = 0, S_z = 1$ amplitude has the form

$$M^{(0,+)}_{\uparrow\uparrow} \propto \frac{mk_\perp e^{-i\phi}}{k_\perp^2 + m^2}\,, \tag{19}$$

while for $J_z = 2, S_z = 0, P = +1$, we have

$$M_{\uparrow\downarrow}^{(2,+)} \propto \frac{-k_\perp^2 (ze^{i2\phi} - (1-z)e^{-i2\phi})}{k_\perp^2 + m^2}, \tag{20}$$

which does not vanish as $m \to 0$. Indeed, in the massless case only amplitudes for $J_z = \pm 2, S_z = 0$ with $L_z = \pm 2$ contribute. The amplitudes in this case enter the cross section as

$$\begin{aligned}\sum_{\lambda\bar\lambda} M_{ik}^{\lambda\bar\lambda} M_{jl}^{\lambda\bar\lambda\dagger} \quad &\Longrightarrow \quad P_{ik}^{\|} P_{jl}^{\|} \sum_{\lambda=-\bar\lambda} \left| M_{\lambda\bar\lambda}^{(2,-)} \right|^2 + P_{ik}^{\perp} P_{jl}^{\perp} \sum_{\lambda=-\bar\lambda} \left| M_{\lambda\bar\lambda}^{(2,+)} \right|^2 \\ &= \quad \frac{2}{k_\perp^2} \Big\{ \frac{z^2 + (1-z)^2}{z(1-z)} \Big(P_{ik}^{\|} P_{jl}^{\|} + P_{ik}^{\perp} P_{jl}^{\perp} \Big) \\ &+ \quad 2\cos(4\phi) \Big(P_{ik}^{\|} P_{jl}^{\|} - P_{ik}^{\perp} P_{jl}^{\perp} \Big) \Big\}\end{aligned}$$

We observe, that at the cross section level, the $L_z = \pm 2$ amplitudes give rise to a $\cos(4\phi)$ modulation. It gives rise to a difference between $\|$ and $\perp$ linear polarizations of "s-channel" photons. As the cross section is the absorptive part of a forward amplitude, which in turn can be related to an index of refraction, one can indeed relate this to a "birefringence" of the vacuum, see the discussion in Ref. [21]. Furthermore, from the Fierz transformation

$$\begin{aligned}\Big(P^{\|} \otimes P^{\|} + P^{\perp} \otimes P^{\perp} \Big) \Big|_{s-\text{channel}} &= \Big(\mathbb{I} \otimes \mathbb{I} - \varepsilon \otimes \varepsilon \Big) \Big|_{t-\text{channel}} \\ \Big(P^{\|} \otimes P^{\|} - P^{\perp} \otimes P^{\perp} \Big) \Big|_{s-\text{channel}} &= \Big(P^{\|} \otimes P^{\|} - P^{\perp} \otimes P^{\perp} \Big) \Big|_{t-\text{channel}},\end{aligned} \tag{21}$$

one can derive, that in the $\boldsymbol{b}$-integrated cross section, the $\cos(4\phi)$ modulation stems from the linearly polarized TMD $h_1^\perp(x, q_\perp^2)$ as previously shown in Ref.[22]. In the massive case, relevant to invariant masses close to the threshold, **interferences** between $J_z = 0$ and $J_z = \pm 2$ amplitudes of equal parity can induce a $\cos(2\phi)$ modulation.

$$\begin{aligned}\sum_{\lambda\bar\lambda} M_{ik}^{\lambda\bar\lambda} M_{jl}^{\lambda\bar\lambda\dagger} \quad \supset \quad & \delta_{ik} P_{jl}^{\|} \sum_{\lambda\bar\lambda} M_{\lambda\bar\lambda}^{(0,+)} M_{\lambda\bar\lambda}^{(2,+)\dagger} + P_{ik}^{\|} \delta_{jl} \sum_{\lambda\bar\lambda} M_{\lambda\bar\lambda}^{(2,+)} M_{\lambda\bar\lambda}^{(0,+)\dagger} \\ + \quad & \epsilon_{ik} P_{jl}^{\perp} \sum_{\lambda\bar\lambda} M_{\lambda\bar\lambda}^{(0,-)} M_{\lambda\bar\lambda}^{(2,-)\dagger} + P_{ik}^{\perp} \epsilon_{jl} \sum_{\lambda\bar\lambda} M_{\lambda\bar\lambda}^{(2,-)} M_{\lambda\bar\lambda}^{(0,-)\dagger}\end{aligned} \tag{22}$$

We can expect a different dependence on centrality the $\cos 2\phi$ and $\cos 4\phi$ contributions. In the $\boldsymbol{b}$–integrated cross section the $\cos 2\phi$ stems from the product of unpolarized & linearly polarized TMD's: $f_1(x_1, q_{1\perp}^2) h_1^\perp(x_2, q_{2\perp}^2) + (x_1, q_{1\perp} \leftrightarrow x_2, q_{2\perp})$, in agreement with the analysis in Ref.[22].

2.5 Comparison with STAR data

$\sqrt{s_{NN}} = 200\,\text{GeV}$	Wigner	Wigner	STAR	STAR
centrality	A_4	$\sqrt{\langle P_T^2 \rangle}$ MeV	$\lvert A_4 \rvert$	$\sqrt{\langle P_T^2 \rangle}$ MeV
60-80 %	-0.39	47.7	0.27 ± 6	50.9 ± 2.5
40-60 %	-0.49	51.0	–	–
20-40 %	-0.62	54.8	-	-
0-20%	-0.77	59.6	-	-

Table 1: Centrality dependence of angular coefficient and mean P_T of e^+e^--pair.

Let us now go to the comparison with experimental data. Here we define, event by event, the x-axis in the transverse plane to be along $\boldsymbol{P} = \boldsymbol{p}_+ + \boldsymbol{p}_-$, so that the internal orbital angular momenta of leptons reflect themselves in a modulation in the angle:

$$\cos\phi = \frac{\boldsymbol{P} \cdot (\boldsymbol{p}_- - \boldsymbol{p}_+)}{|\boldsymbol{P}||\boldsymbol{p}_- - \boldsymbol{p}_+|} \approx \frac{\boldsymbol{P} \cdot \boldsymbol{k}}{|\boldsymbol{P}||\boldsymbol{k}|},. \tag{23}$$

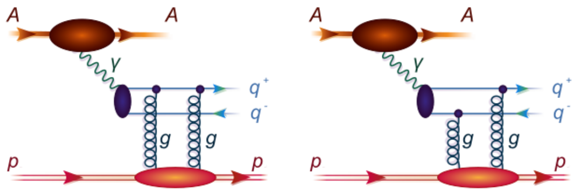

Figure 5 – Feynman diagrams for the diffractive photoproduction of $q\bar{q}$ pairs in nucleus-proton collisions, discussed in the present paper.

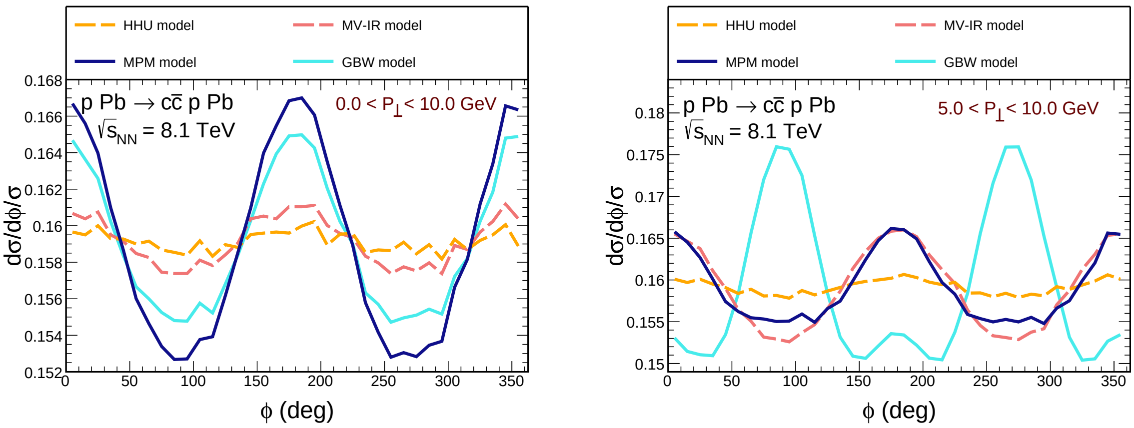

Figure 6 – Distributions in the azimuthal angle ϕ between $\vec{P}_\perp$ and $\vec{\Delta}_\perp$ normalised to the total cross section for $0.01 < P_\perp < 10.0\,\text{GeV}$ on the left and for $5.0 < P_\perp < 10.0\,\text{GeV}$ on the right.

A comparison with STAR[20] data in the $60-80\%$ centrality class, which show a sizable, negative $\cos(4\phi)$ modulation, is seen in Fig.4. The angular modulation clearly reflects the orbital angular momentum $L_z = \pm 2$ of leptons. The agreement with data is good, we stress that no new parameters enter the calculation. In Table 1 we show the A_4 correlation coefficient in

$$\frac{dN}{d\phi} \propto 1 + A_2 \cos 2\phi + A_4 \cos 4\phi + \dots. \tag{24}$$

In particular we predict its evolution with centrality: an increasing in size, and negative azimuthal correlation A_4.

3 Diffractive photoproduction of $c\bar{c}$ pairs

Finally, let us return to the gluon Wigner distribution/GTMD. Here, also ultraperipheral collisions have been proposed as a means to gain access to the latter [23,24]. We briefly summarize the main results of our recent paper[25] regarding the azimuthal correlations of diffractively produced $c\bar{c}$-pairs. Here we have in mind UPC in proton-nucleus collisions, where the nucleus provides the photon flux and the diffractive photoproduction process proceeds on the proton (see Fig.5). The photoproduction amplitude in the dipole picture is expresed as

$$\frac{d\sigma(\gamma p \to Q\bar{Q}p; s_{\gamma p})}{dz d^2\boldsymbol{P} d^2\boldsymbol{\Delta}} = \overline{\sum_{\lambda_\gamma,\lambda,\bar{\lambda}}} \Big| \int \frac{d^2\boldsymbol{b} d^2\boldsymbol{r}}{(2\pi)^2} e^{-i\boldsymbol{\Delta}\cdot\boldsymbol{b}} e^{-i\boldsymbol{P}\cdot\boldsymbol{r}} N(Y,\boldsymbol{r},\boldsymbol{b})\, \Psi^{\lambda_\gamma}_{\lambda\bar{\lambda}}(z,\boldsymbol{r}) \Big|^2 . \tag{25}$$

Now, one is interested in the azimuthal correlation in the angle

$$\cos\phi = \frac{\boldsymbol{P}\cdot\boldsymbol{\Delta}}{P_\perp \Delta_\perp} \tag{26}$$

Indeed, a possible correlation between dipole size $\boldsymbol{r}$ and impact parameter $\boldsymbol{b}$ reflects itself in an angular correlation in the GTMD (the so-called "elliptic GTMD".

$$f\Big(Y, \frac{\boldsymbol{q}}{2} + \boldsymbol{\kappa}, \frac{\boldsymbol{q}}{2} - \boldsymbol{\kappa}\Big) = f_0(Y, \kappa_\perp, q_\perp) + 2\cos(2\phi_{q\kappa})\, f_2(Y, \kappa_\perp, q_\perp)\,. \tag{27}$$

Here Y is the rapidity gap between diffractive system and proton, and the gluon GTMD relates to the dipole amplitude as

$$\begin{aligned} N(Y, \boldsymbol{r}, \boldsymbol{b}) &= \int d^2\boldsymbol{q} d^2\boldsymbol{\kappa}\, f\Big(Y, \frac{\boldsymbol{q}}{2} + \boldsymbol{\kappa}, \frac{\boldsymbol{q}}{2} - \boldsymbol{\kappa}\Big) \exp[i\vec{q}_\perp \cdot \vec{b}_\perp] \\ &\times \Big\{ \exp\Big[i\frac{1}{2}\boldsymbol{q}\cdot\boldsymbol{r}\Big] + \exp\Big[-i\frac{1}{2}\boldsymbol{q}\cdot\boldsymbol{r}\Big] - \exp[i\boldsymbol{\kappa}\cdot\boldsymbol{r}] - \exp[-i\boldsymbol{\kappa}\cdot\boldsymbol{r}] \Big\}\,. \end{aligned} \tag{28}$$

In this case, the dominant correlation turns out to be $\cos 2\phi$, and it inded stems from the "elliptic glue". The size of the effect shown in Fig.6 however is much smaller than the one in photon-photon fusion production for the dilepton.

4 Summary

We have reviewed our studies of low-P_T dilepton production in ultrarelativistic heavy-ion collisions. We first performed a comparison of dilepton production via thermal radiation and photon-photon fusion within the coherent fields of the incoming nuclei. Coherent emission dominates for the two peripheral samples, and is comparable to the cocktail and thermal radiation yields in semi-central collisions. The impact-parameter dependent dilepton P_T distribution is described by a Wigner function density matrix generalization of the Weizsäcker-Williams fluxes. Here the $J_z = 0, \pm 2$ channels of the $\gamma\gamma$-system enter with different $\boldsymbol{b}$-dependent weights. For e^+e^- pairs the $J_z = \pm 2$ channels dominate. Comparison to recent STAR data shows a good description of low-P_T dilepton data in Au-Au($\sqrt{s_{NN}}$=200 GeV) collisions in three centrality classes, for invariant masses from threshold to $\sim$4 GeV. Proper account for the b-dependence turns out to be crucial at LHC energies. We obtain a very good description of ATLAS azimuthal decorrelations, our predictions agree well with recent ALICE data.

Also the azimuthal $\cos 4\phi$ correlation measured by STAR is well reproduced, and can be traced to orbital angular momentum of leptons. Here the linear photon polarizations play an important role. The angular coefficient rises for more central collisions.

In contrast, in diffractive heavy quark production, the parton-level $\cos 2\phi$ azimuthal correlations induced by the elliptic Wigner function are much smaller than the ones in the QED process.

Acknowledgments

It is a pleasure to thank the organizers for the invitation to this topical workshop, which brought back fond memories of Gerhard Baur's kindness and encouragement. I hope he would have liked the results presented here. This work was partially supported by the Polish National Science Center grant UMO-2018/31/B/ST2/03537.

References

1. Carlos A. Bertulani and Gerhard Baur. Electromagnetic Processes in Relativistic Heavy Ion Collisions. *Phys. Rept.*, 163:299, 1988.
2. Carlos A. Bertulani, Spencer R. Klein, and Joakim Nystrand. Physics of ultra-peripheral nuclear collisions. *Ann. Rev. Nucl. Part. Sci.*, 55:271–310, 2005.
3. J.G. Contreras and J.D. Tapia Takaki. Ultra-peripheral heavy-ion collisions at the LHC. *Int. J. Mod. Phys. A*, 30:1542012, 2015.
4. Wolfgang Schäfer. Photon induced processes: from ultraperipheral to semicentral heavy ion collisions. *Eur. Phys. J. A*, 56(9):231, 2020.
5. N. Baron and G. Baur. Unraveling gamma gamma dileptons in central relativistic heavy ion collisions. *Z. Phys. C*, 60:95–100, 1993.
6. Jaroslav Adam et al. Measurement of an excess in the yield of J/ψ at very low $p_{\rm T}$ in Pb-Pb collisions at $\sqrt{s_{\rm NN}} = 2.76$ TeV. *Phys. Rev. Lett.*, 116(22):222301, 2016.
7. Jaroslav Adam et al. Low-p_T e^+e^- pair production in Au+Au collisions at $\sqrt{s_{NN}} = 200$ GeV and U+U collisions at $\sqrt{s_{NN}} = 193$ GeV at STAR. *Phys. Rev. Lett.*, 121(13):132301, 2018.

8. Sebastian Lehner. Dielectron production at low transverse momentum in Pb-Pb collisions at $\sqrt{s_{\mathrm{NN}}} = 5.02$ TeV with ALICE. *PoS*, LHCP2019:164, 2019.
9. Mariola Kłusek-Gawenda, Ralf Rapp, Wolfgang Schäfer, and Antoni Szczurek. Dilepton Radiation in Heavy-Ion Collisions at Small Transverse Momentum. *Phys. Lett. B*, 790:339–344, 2019.
10. Ralf Rapp. Dilepton Spectroscopy of QCD Matter at Collider Energies. *Adv. High Energy Phys.*, 2013:148253, 2013.
11. Spencer R. Klein, Joakim Nystrand, Janet Seger, Yuri Gorbunov, and Joey Butterworth. STARlight: A Monte Carlo simulation program for ultra-peripheral collisions of relativistic ions. *Comput. Phys. Commun.*, 212:258–268, 2017.
12. Mariola Kłusek-Gawenda, Wolfgang Schäfer, and Antoni Szczurek. Centrality dependence of dilepton production via $\gamma\gamma$ processes from Wigner distributions of photons in nuclei. *Phys. Lett. B*, 814:136114, 2021.
13. Spencer Klein, A. H. Mueller, Bo-Wen Xiao, and Feng Yuan. Lepton Pair Production Through Two Photon Process in Heavy Ion Collisions. *Phys. Rev. D*, 102(9):094013, 2020.
14. M. Vidovic, M. Greiner, C. Best, and G. Soff. Impact parameter dependence of the electromagnetic particle production in ultrarelativistic heavy ion collisions. *Phys. Rev. C*, 47:2308–2319, 1993.
15. Kai Hencken, Gerhard Baur, and Dirk Trautmann. Production of QED pairs at small impact parameter in relativistic heavy ion collisions. *Phys. Rev. C*, 69:054902, 2004.
16. Cong Li, Jian Zhou, and Ya-Jin Zhou. Impact parameter dependence of the azimuthal asymmetry in lepton pair production in heavy ion collisions. *Phys. Rev. D*, 101(3):034015, 2020.
17. Roman Pasechnik and Marek Taševský. Multi-dimensional hadron structure through the lens of gluon Wigner distribution, hep-ph2310.10793. 10 2023.
18. Georges Aad et al. Measurement of muon pairs produced via $\gamma\gamma$ scattering in nonultraperipheral Pb+Pb collisions at sNN=5.02 TeV with the ATLAS detector. *Phys. Rev. C*, 107(5):054907, 2023.
19. Daniël Boer, Tom Van Daal, Piet J. Mulders, and Elena Petreska. Directed flow from C-odd gluon correlations at small x. *JHEP*, 07:140, 2018.
20. Jaroslav Adam et al. Measurement of e^+e^- Momentum and Angular Distributions from Linearly Polarized Photon Collisions. *Phys. Rev. Lett.*, 127(5):052302, 2021.
21. James Daniel Brandenburg, Janet Seger, Zhangbu Xu, and Wangmei Zha. Report on progress in physics: observation of the Breit–Wheeler process and vacuum birefringence in heavy-ion collisions. *Rept. Prog. Phys.*, 86(8):083901, 2023.
22. Cong Li, Jian Zhou, and Ya-Jin Zhou. Probing the linear polarization of photons in ultraperipheral heavy ion collisions. *Phys. Lett. B*, 795:576–580, 2019.
23. Yoshikazu Hagiwara, Yoshitaka Hatta, Roman Pasechnik, Marek Tasevsky, and Oleg Teryaev. Accessing the gluon Wigner distribution in ultraperipheral pA collisions. *Phys. Rev. D*, 96(3):034009, 2017.
24. Mateus Reinke Pelicer, Emmanuel Gräve De Oliveira, and Roman Pasechnik. Exclusive heavy quark-pair production in ultraperipheral collisions. *Phys. Rev. D*, 99(3):034016, 2019.
25. Barbara Linek, Agnieszka Łuszczak, Marta Łuszczak, Roman Pasechnik, Wolfgang Schäfer, and Antoni Szczurek. Probing proton structure with $c\bar{c}$ correlations in ultraperipheral pA collisions. *JHEP*, 10:179, 2023.